EUROPEAN COMMISSION

Community research

PAMINA
Performance Assessment Methodologies in Application to Guide the Development of the Safety Case

(Contract Number: FP6-036404)

A Hydrogeochemical Change in an Engineered Barrier System – Two Model Responses to Uranium Transport
DELIVERABLE (D-N°: D2.2.B.3)

Author(s): **Ari Luukkonen and Henrik Nordman**
Technical Research Centre of Finland (VTT)

Date of issue of this report : **17/06/2008**

Start date of project : **01/10/2006** Duration : 36 Months

Project co-funded by the European Commission under the Euratom Research and Training Programme on Nuclear Energy within the Sixth Framework Programme (2002-2006)		
Dissemination Level		
PU	Public	X
RE	Restricted to a group specified by the partners of the [PAMINA] project	
CO	Confidential, only for partners of the [PAMINA] project	

Foreword

The work presented in this report was developed within the Integrated Project PAMINA: **P**erformance **A**ssessment **M**ethodologies **IN A**pplication to Guide the Development of the Safety Case. This project is part of the Sixth Framework Programme of the European Commission. It brings together 25 organisations from ten European countries and one EC Joint Research Centre in order to improve and harmonise methodologies and tools for demonstrating the safety of deep geological disposal of long-lived radioactive waste for different waste types, repository designs and geological environments. The results will be of interest to national waste management organisations, regulators and lay stakeholders.

The work is organised in four Research and Technology Development Components (RTDCs) and one additional component dealing with knowledge management and dissemination of knowledge:

- In RTDC 1 the aim is to evaluate the state of the art of methodologies and approaches needed for assessing the safety of deep geological disposal, on the basis of comprehensive review of international practice. This work includes the identification of any deficiencies in methods and tools.

- In RTDC 2 the aim is to establish a framework and methodology for the treatment of uncertainty during PA and safety case development. Guidance on, and examples of, good practice will be provided on the communication and treatment of different types of uncertainty, spatial variability, the development of probabilistic safety assessment tools, and techniques for sensitivity and uncertainty analysis.

- In RTDC 3 the aim is to develop methodologies and tools for integrated PA for various geological disposal concepts. This work includes the development of PA scenarios, of the PA approach to gas migration processes, of the PA approach to radionuclide source term modelling, and of safety and performance indicators.

- In RTDC 4 the aim is to conduct several benchmark exercises on specific processes, in which quantitative comparisons are made between approaches that rely on simplifying assumptions and models, and those that rely on complex models that take into account a more complete process conceptualization in space and time.

The work presented in this report was performed in the scope of RTDC 2.

All PAMINA reports can be downloaded from http://www.ip-pamina.eu.

A HYDROGEOCHEMICAL CHANGE IN AN ENGINEERED BARRIER SYSTEM – TWO MODEL RESPONSES TO URANIUM TRANSPORT

Deliverable D2.2B.3
June 17th, 2008

Ari Luukkonen
Henrik Nordman
VTT Technical Research Centre of Finland
P.O.BOX 1000
FIN-02044 VTT

ABSTRACT

Nuclear repository performance calculations, considering potential radionuclide transport are classically done utilising distribution coefficients. Distribution coefficients are based on experimental field data or laboratory experiments and calculations give estimates on average nuclide retardation within engineered barrier system and also within bedrock. Distribution coefficients are used to simplify complex problems and coefficients defined conservatively (higher nuclide transport predicted than probable). Distribution coefficient based retardation modelling approach, however, usually fails to describe system changes and more mechanistic approaches that the divide lumped system into smaller subsystems has to be considered.

Current study compares results of distribution coefficient based retardation approach and a mechanistic approach that utilises coupled reactive transport. The system change induced is a moving redox front within the studied system and calculations concentrate to uranium transport. Uranium transport is strongly redox sensitive. In the oxic conditions uranium is highly soluble, while in the reducing conditions uranium is effectively retarded in the solid phases.

The calculations show that the differences in results between the two methods are quite remarkable. The distribution coefficient based calculations indicate conservatively that uranium transport is much higher and breakthrough of uranium occurs much earlier than in the case of coupled reactive transport calculations. Interestingly, however, reactive transport calculations predict that there may be quite high dissolved uranium concentrations within the studied pathway, though practically no uranium comes through. When the breakthrough occurs in the reactive transport simulation, extensive amounts of uranium are suddenly moving.

Some of the highlights and drawbacks of both modelling methods are summarised. Both modelling methods are vital tools for performance assessment calculations.

1 INTRODUCTION

Understanding the radionuclide transport and retardation within the geological and engineered barriers is among the important issues in performance assessment analyses assigned for final repositories of spent nuclear fuel. The rationale for studies is based on various potential canister failure scenarios and what happens to nuclides released from failed canisters. Usually, two different approaches can be used to describe the partitioning of radionuclides between geological and/or engineered solids, and solutions at equilibrium conditions:

1) Lumped retardation approach (K_d) that have been "conservatively" estimated from experimental field data or laboratory experiments.

2) Models based on theoretical considerations describing interaction processes in a mechanistic manner.

Because of complexity of natural systems, the empirical K_d approach has been widely used in describing the partitioning of solutes between solid and liquid phases. Especially, this holds for the aerial scale transport modelling studies. However, the mechanistic approach has gained more popularity among laboratory investigators, since modelling targets to thermodynamical understanding of individual geochemical processes.

The empirical retardation approaches usually fail to model the change within the hydrogeochemical system. In the case of distribution coefficient (K_d) based modelling, the changes in pH, temperature, background electrolyte composition and concentration, concentrations of competing adsorbates, and redox sensitive processes are omitted. Consequently, the distribution coefficient based predictions related to system changes have usually little value.

However, the mechanical approach has its drawbacks as well. The approach is based on hydro- and thermodynamics, and is able to response to system changes. Consequently, the model may need a lot of hydraulic and thermodynamic parameters, and the model structure may become very complex. Often, all the parameterisation cannot be verified and the utilisation is based on reasonable assumptions.

Nevertheless, the current study attempts to make a comparison between the two approaches. The exercise considers uranium transport. Uranium (^{238}U) was chosen because it is redox and to a degree pH sensitive element. Mechanistic calculations are made for conditions where redox (and pH) conditions change during simulation. The used hydraulic parameterisation and some of the water composition assumptions are simply examples, though they may be loosely assigned to real Olkiluoto scenarios. However, the following comparison is an exercise that only attempts to demonstrate differences between distribution coefficients and mechanistic based modelling approaches.

2 CONCEPTUAL MODEL AND CALCULATION TOOLS

To assess the geochemical environment of groundwater and solutes at the canister scale, the repository is conceptualized as series of unit cells. A unit cell comprises a section of the deposition tunnel (backfilled), the buffer and canister in the deposition hole (Figure 2-1).

The unit cell is composed of a 5.5-metre long section of tunnel (77 m^3) and of one deposition hole (19 m^3). The volume of the unit cell is 96 m^3. The tunnel backfill consists of 30% MX-80 sodium bentonite mixed with 70% crushed rock. The deposition hole contains the spent fuel canister and compacted bentonite blocks. For a full-scale test of the KBS-3V repository concept, Börgesson & Hernelind (1999) have estimated general physical properties for a tunnel backfill (Table 2-1).

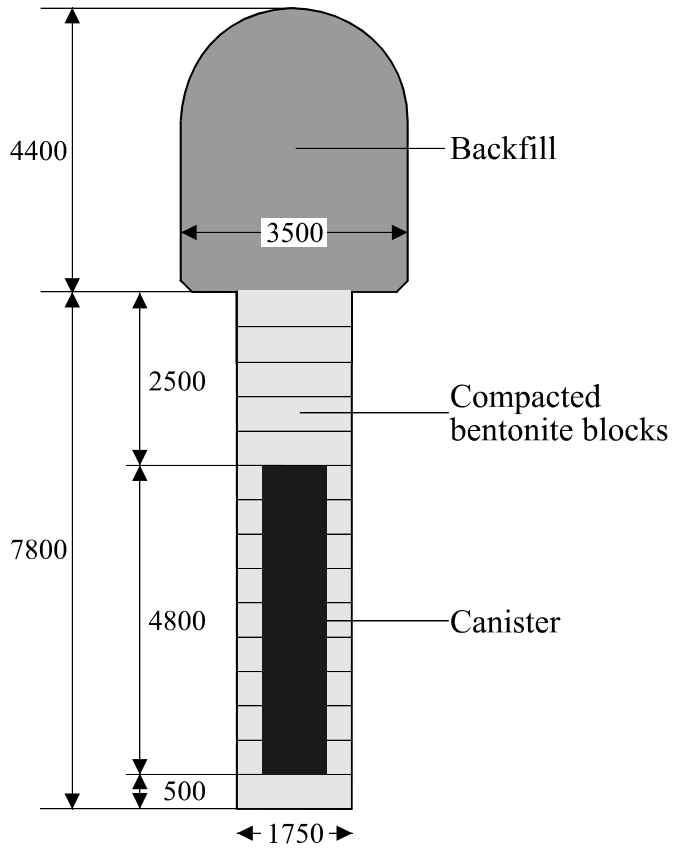

Figure 2-1. *Dimensions of the deposition hole and part of the deposition tunnel used in the conceptual model of the unit cell. All measures presented are in millimetres.*

Table 2-1. *Selected physical properties for initial compacted tunnel backfill in the Prototype repository (Äspö, Sweden). Parameters are after Börgesson & Hernelind (1999). Water content (m_{water}/m_{solid}), porosity (V_{void}/V_{tot}), and degree of saturation (V_{water}/V_{void}).*

Dry density g/cm^3	Water content	Porosity	Degree of saturation
1.75	0.19	0.363	0.58

In the classical retardation/diffusion model applied in REPCOM the retardation factor R of backfill is the relationship of total amount of species per amount dissolved in water. The R is obtained from equation 2-1 as:

$$R = 1 + \frac{(1-\varepsilon)\rho_g K_d}{\varepsilon} \ , \qquad \text{(Equation 2-1)}$$

where

R is the retardation factor of the species in the backfill (-),

ε is the porosity of the backfill (0.363)

K_d is the volume-based distribution coefficient (0.15 m^3/kg for uranium),

ρ_g is grain dry density of the backfill (2750 kg/m^3), which is dry density of backfill from Table 2–1 per volume of solids.

In REPCOM modelling the above retardation equation has been applied (Nordman & Vieno 1994) The diffusion in backfill takes place according to standard Fick's law and advection is included.

The calculation tool for the geochemical evolution in the deposition tunnel is PHREEQC-2, a modelling tool developed by USGS (Parkhurst & Appelo 1999). In principle, PHREEQC-2 can be applied to simulate the chemistry in the deposition tunnel assuming that a flow of porewater along the tunnel axis can be approximated with a slow advection. The code is capable of taking into account the advective transport of dissolved species undergoing chemical reactions in saturated groundwater system. The code capabilities include modelling of complex sets of reversible reactions, such as aqueous, mineral, gas, solid-solution, surface-complexation, and ion-exchange equilibria, and irreversible reactions, such as specified mole transfers of reactants, kinetically controlled reactions, and mixing of solutions.

It is assumed that bentonite utilised in the tunnel EBS is MX-80 sodium bentonite. The estimated average composition of tunnel backfill is presented in Table 2-2. In the reactive transport calculations, from this set of minerals only pyrite, calcite, goethite, and amorphous iron are considered reactive in the current study. However, amorphous iron is a metastable mineral phase, and tends to recrystallise as goethite. These two mineral phases were summed up as goethite in the calculations.

In the reactive transport calculations also cation exchange and surface complexation processes are assumed to be effective. The amounts of cation exchange and surface complexation sites tabulated in Table 2-2 are in accordance with Bradbury & Baeyens (2002, 2005). It is assumed that only the bentonite component (30%) of the backfill mixture contributes to the cation exchange and surface complexation site capacities.

Table 2-2. *Potentially reactive solids of the Olkiluoto repository tunnel backfill.*

	[a)] Ecoclay II Crshed rock Ave	[b)] B & B Bentonite MX-80	70/30 Mix	70/30 Mix 4821.25 g
Minerals	**mol/g**	**mol/g**	**mol/g**	**mol**
Quartz	3.87E-03	2.50E-03	3.46E-03	16.666
Montmorillonite		1.01E-03	3.02E-04	1.458
Oligoclase-Albite	7.24E-04	2.29E-04	5.75E-04	2.773
Microcline	6.18E-04		4.32E-04	2.085
Biotite	4.62E-04		3.24E-04	1.560
Cordierite	1.38E-04		9.69E-05	0.467
Sillimanite	3.30E-04		2.31E-04	1.115
CH_2O		1.33E-04	4.00E-05	0.193
Musc./Sericite	7.25E-05		5.08E-05	0.245
Chlorite/Hornbl.	2.26E-05		1.58E-05	0.076
Zircon	1.47E-05		1.03E-05	0.050
Kaolinite		2.71E-05	8.13E-06	0.039
Illite		9.00E-06	2.70E-06	0.013
Epid./Sauss.	6.07E-06		4.25E-06	0.020
Cc-Dol	1.20E-05	6.52E-05	2.79E-05	0.135
Siderite		6.52E-05	1.96E-05	0.094
Apatite	1.58E-06		1.11E-06	0.005
Garnet	9.72E-07		6.80E-07	0.003
Pyrite	2.40E-05	2.50E-05	2.43E-05	0.117
Pyrrhotite	5.00E-06		3.50E-06	0.017
Graphite	4.15E-05		2.90E-05	0.140
Halite		1.35E-06	4.05E-07	0.002
Gypsum		2.35E-05	7.05E-06	0.034
Goethite		1.53E-05	4.59E-06	0.022
Molybdenite	9.86E-07		6.90E-07	0.003
Galena	7.08E-07		4.96E-07	0.002
Occupancies in the exchange sites		**mol/g**	**mol/g**	**mol**
Ca^{2+}		3.30E-05	9.90E-06	0.048
Mg^{2+}		2.00E-05	6.00E-06	0.029
Na^{+}		6.68E-04	2.00E-04	0.966
K^{+}		1.30E-05	3.90E-06	0.019
Surface site capacities		**mol/g**	**mol/g**	**mol**
$S^{s}OH$		2.0E-06	6.0E-07	0.003
$S^{w1}OH$		4.0E-05	1.2E-05	0.058
$S^{w2}OH$		4.0E-05	1.2E-05	0.058

[a)] *General mineral composition after Vuorinen et al. (2003).*

[b)] *General mineral composition after Bradbury & Baeyens (2002), exchange occupancies after Bradbury & Baeyens (2003), and surface site capacities after Bradbury & Baeyens (2005).*

2.1 Water compositions

The water compositions considered in the calculations are presented in Table 2-3. The tunnel backfill is initially filled with anoxic brackish porewater equilibrated with calcite, goethite, and pyrite. The exchange sites of the backfill are equilibrated with this water at the beginning of calculations. Initial porewater is essentially inert considering the tunnel backfill. The salinity of initial porewater is based on the salinity levels that prevail at present in the repository depth at the Olkiluoto site.

The composition of dilute infiltrating water is based on an actual meteoric water composition sampled (Sample PP5_2, TDS 85.5 mg/L) from the Olkiluoto Island. However, the actual water composition is equilibrated with goethite before passing the water into reactive transport calculations. Infiltrating water contains a moderate amount of dissolved O_2 (3.0 mg/L). Its redox value is strongly oxic and water is capable to dissolve and transport uranium (as U^{6+}). It is assumed that infiltrating water contains 0.15 mg/L dissolved uranium.

The calculation exercise loosely imitates e.g. future repository conditions where dilute oxic glacial melt waters are able to penetrate from ground surface to the repository depth. However, calculations attempt to demonstrate differences between reactive transport considerations and lumped parameter approximations (K_d values). Therefore, the consideration is in many respects unlikely. The potential future scenarios and hydraulic properties assigned for the Olkiluoto repository (Cedercreutz 2004, Posiva 2007) differ significantly in many respects from the calculation parameters presented within this work.

Table 2-3. *Water compositions in mg/L considered in the calculations.*

	pH	pe	O_2	C	Ca	Cl	Fe	K	Mg	Na	S	Si	U
Initial Porewater	6.9	-3.2	0.0	17.0	744	6020	0.04	42.8	85.3	2543	71.9	12.3	0.0
Infiltrating Water	4.5	14.5	3.0	1.93	3.0	14.8	0.0	1.75	3.18	3.41	4.34	17.2	0.15

3 HYDROGEOCHEMICAL MODEL FOR THE TUNNEL BACKFILL

The conceptual model used for geochemical calculations in the tunnel part of the unit cell considers slow groundwater flow along the repository tunnel axis. The reactive transport calculations are monitored on the cell-by-cell basis as a function of time. The tunnel unit is divided into 714 columns, and each tunnel backfill column is divided into 39 cells. Calculations are done for one backfill column and the results can be multiplied by 714 if total tunnel volume is considered. In a backfill column porewater is transported through successive backfill cells. An illustration of the modelling is presented in Figure 3-1. The calculation starts from the left (cell #1). Water remains in a cell until the residence time is reached and then the water is transported into next cell further along the tunnel backfill column. The size of an individual tunnel backfill cell is 2.75 dm^3 assuming a porewater volume of 1 dm^3 and a porosity of 0.363 (Table 2-1). The cell is a cube with an edge length of 0.14 metres. The calculation implements the pure 1-D advection without any side diffusion. The flow rate along the individual cell column is 4.2 L/year that corresponds to 3000 L/year in the complete tunnel part considered.

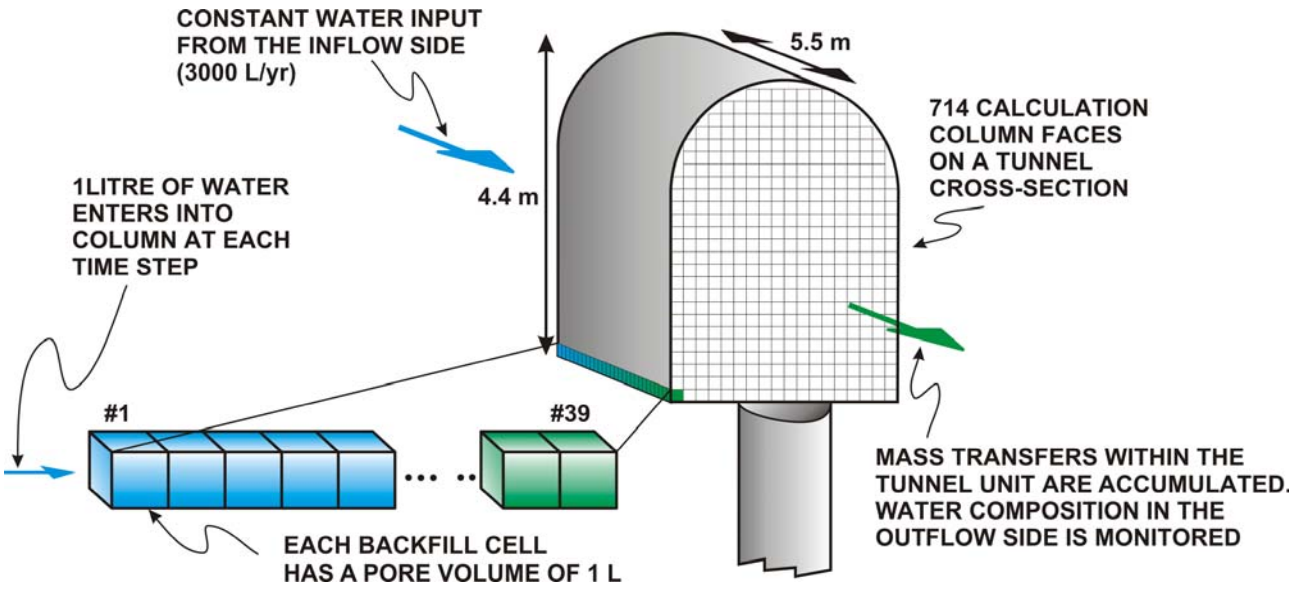

Figure 3-1. *Illustration of the conceptual model of the tunnel backfill part of the unit cell. Infiltrating water moves along the 5.5 metre-long tunnel section of the unit cell. The volume of the tunnel unit is divided into 714 columns. Each calculation column is divided into 39 cells. Material properties for each cell are considered as known parameters (i.e. amounts of reactive materials, cation exchange capacity, and 1-litre pore volume). The volumetric flow rate is assumed to be distributed homogeneously over the tunnel cross-section. Therefore, the flow rate within one calculation column is 1/714th of the total volumetric flow (i.e. 3000 [L/yr] / 714 = 4.2 [L/yr] in one calculation column).*

The length of the tunnel in the unit cell (5.5 metres) was chosen because it corresponds to half the distance between two deposition holes (for OL-1 and OL-2 type of waste). The complete pore volume in the tunnel unit is 27,846 litres (27.8 m^3).

The assumption that water flows along the tunnel axis is simplistic, as other directions are also possible. However, the hydraulic conductivity measurements from a full size tunnel backfilling experiment indicate that hydraulic conductivities within the compacted backfill are clearly higher than within the surrounding normally fractured bedrock (SKB 2005). Therefore, it is likely that water will flow axially along the tunnel. Moreover, the tunnel backfilling experiment (SKB 2005) indicates that hydraulic conductivities within the tunnel backfill vary significantly. The central parts of the tunnel backfill are less conductive than the parts closer to tunnel walls. Finally, the calculation approach yields feasible estimates of the mass transfers irrespective of the direction of flow: considering the dimensions of the unit cell (Figures 2-1 and 3-1) the distances from the top to the bottom (4.4 metres), and from the side wall to the other (3.5 metres) of the tunnel unit are almost the same as the length of the tunnel unit (5.5 metres).

The main geochemical processes occurring in the backfill bentonite are aqueous speciation, mineral equilibria, cation exchange, and surface complexation.

3.1 Aqueous speciation

With the exception of U, aqueous speciation of dissolved species follows the thermodynamic data given in PHREEQC database (delivered with PHREEQC version 2.14.03). Aqueous speciation of uranium follows thermodynamics given by NEA (Grenthe et al. 2004), and by Bradbury & Baeyens (2005). In the case of duplicate information, values delivered by Bradbury & Baeyens (2005) have been used.

3.2 Mineral equilibria

The average mineral composition of the tunnel backfill is presented in Table 2-2. Equilibrium thermodynamics of calcite, pyrite, and iron (amorphous iron and its recrystallised form, goethite) are considered in reactive transport calculations. From the set of possible U minerals, uraninite is taken as potential precipitating U phase (with supersaturation gap SI > 0.5).

3.3 Cation exchange and surface complexation

The thermodynamic constants for cation exchange and surface complexation equilibria are presented on Table 3-1. The exchange and surface site capacities are presented in Table 2-2. The cation exchange equilibria are after Bradbury & Baeyens (2003), but are supplemented with Fe exchange equilibrium after Charlet & Tournassat (2005). The surface complexation thermodynamics follows the equilibria given by Bradbury & Baeyens (2005). At near neutral pH, it is expected that wet clay mineral surfaces e.g. montmorillonite, kaolinite, and illite) become slightly negatively charged (cf. Appelo & Postma, 1996; Davis & Kent, 1990).

Table 3-1. *Exchange and surface parameters for the thermodynamic models considered.*

Parameter	Reaction	Value
	Cation exchange[a]	
log*K*	$Ca^{2+} + 2NaX \Leftrightarrow CaX_2 + 2Na^+$	0.41
log*K*	$Mg^{2+} + 2NaX \Leftrightarrow MgX_2 + 2Na^+$	0.34
log*K*	$K^+ + NaX \Leftrightarrow KX + Na^+$	0.60
log*K*	$Fe^{2+} + 2NaX \Leftrightarrow FeX_2 + 2Na^+$	0.34
	Surface complexation[b]	
log*K*	$\equiv S^SOH + H^+ \Leftrightarrow \equiv S^SOH_2^+$	4.5
log*K*	$\equiv S^SOH \Leftrightarrow \equiv S^SO^- + H^+$	-7.9
log*K*	$\equiv S^SOH + UO_2^{2+} \Leftrightarrow \equiv S^SOUO_2^+ + H^+$	3.1
log*K*	$\equiv S^SOH + UO_2^{2+} + H_2O \Leftrightarrow \equiv S^SOUO_2(OH) + 2H^+$	-3.4
log*K*	$\equiv S^SOH + UO_2^{2+} + 2H_2O \Leftrightarrow \equiv S^SOUO_2(OH)_2^- + 3H^+$	-11.0
log*K*	$\equiv S^SOH + UO_2^{2+} + 3H_2O \Leftrightarrow \equiv S^SOUO_2(OH)_3^{2-} + 4H^+$	-20.5
log*K*	$\equiv S^SOH + U^{4+} \Leftrightarrow \equiv S^SOU^{3+} + H^+$	7.7
log*K*	$\equiv S^SOH + U^{4+} + H_2O \Leftrightarrow \equiv S^SOUOH^{2+} + 2H^+$	7.1
log*K*	$\equiv S^SOH + U^{4+} + 2H_2O \Leftrightarrow \equiv S^SOU(OH)_2^+ + 3H^+$	3.8
log*K*	$\equiv S^SOH + U^{4+} + 3H_2O \Leftrightarrow \equiv S^SOU(OH)_3 + 4H^+$	-2.1
log*K*	$\equiv S^{W1}OH + H^+ \Leftrightarrow \equiv S^{W1}OH_2^+$	4.5
log*K*	$\equiv S^{W1}OH \Leftrightarrow \equiv S^{W1}O^- + H^+$	-7.9
log*K*	$\equiv S^{W1}OH + UO_2^{2+} \Leftrightarrow \equiv S^{W1}OUO_2^+ + H^+$	0.7
log*K*	$\equiv S^{W1}OH + UO_2^{2+} + H_2O \Leftrightarrow \equiv S^{W1}OUO_2(OH) + 2H^+$	-5.7
log*K*	$\equiv S^{W1}OH + U^{4+} \Leftrightarrow \equiv S^{W1}OU^{3+} + H^+$	5.8
log*K*	$\equiv S^{W2}OH + H^+ \Leftrightarrow \equiv S^{W2}OH_2^+$	6.0
log*K*	$\equiv S^{W2}OH \Leftrightarrow \equiv S^{W2}O^- + H^+$	-10.5

[a] According to Bradbury & Baeyens (2003) and Charlet & Tournassat (2005), Gaines-Thomas convention.
[b] According to Bradbury & Baeyens (2005)

4 RESULTS

4.1 Retardation approach with REPCOM model

The obtained concentration profile in backfill with REPCOM model is shown in Figure 4-1. The presented time steps are 1 000 and 10 000 years. After 10 000 years the concentration is 0.15 mg/l in the whole domain.

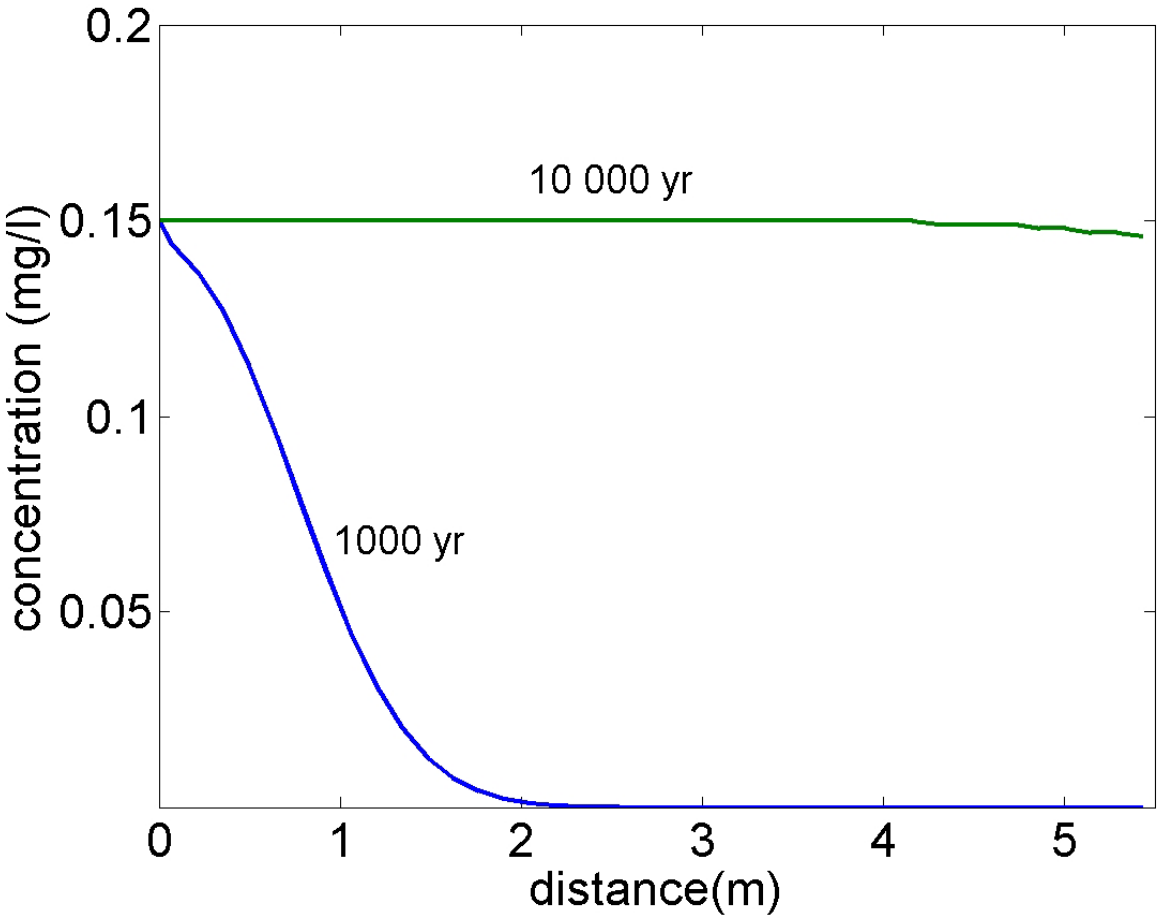

Figure 4-1. *Water phase concentration of uranium with retardation model within the calculation column at selected 1 000 and 10 000 years time steps.*

4.2 Mechanistic approach with PHREEQC

Results presented consider porewater geochemistry within the single calculation column at four different time steps, i.e. 1 000, 10 000, 20 000, and 40 000 years from the beginning of the simulations. The mass transfers assigned to the whole 5.5-metre piece of the tunnel are multiplicative from the results of single column.

Figure 4-2 presents simulated pH and redox evolution within the calculation column as a function of time. At the stage of 1 000 years pH/redox conditions are mostly still in a transient condition. In the distal part of the column (cells #35 – #39, i.e. 4.9m – 5.5m) there is calcite available, and therefore pH is buffered to a relatively high value (around 10). In the mid-part of the column (cells #18 – #34, i.e. 2.5m – 4.8m) there is initial goethite within the column (around 22 mmol/cell, cf. Table 2-2) though calcite is vanished. Since the ionic strength of infiltrating water is low, proton surface complexation (cf. Table 3-1) coupled with small dissolution of goethite is able to raise pH values within porewater to levels around 7.8. The dissolution of goethite consumes protons as follows:

$$FeOOH + 3H^+ \Leftrightarrow Fe^{3+} + 2H_2O\,. \qquad \text{(Equation 4-1)}$$

At the stage of 1 000 years, all cells of the calculation column still contain initial pyrite (cf. Table 2-2). Pyrite is the reactive phase that consumes dissolved oxygen away from the infiltrating solution (cf. Table 2-3). Because pyrite is assumed as an equilibrium phase the redox drop is immediate already in the cell #1. pH and redox values remain at constant low levels until goethite is met after the cell #17 (2.4m). The subsequent raises in pH values enable the redox drops towards more reducing conditions (cf. Figure 4-2). Contemporaneously with the redox drop, dissolved iron vanishes from the solution.

After 10 000, 20 000, and 40 000 simulated years the pyrite front is met in the cells #10 (1.4m), #19 (2.7m), and #38 (5.3m), respectively. Consequently, pe values drop abruptly in these cells. The pyrite dissolution process can be described with following reaction:

$$FeS_2 + 7/2\,O_2 + H_2O \Rightarrow Fe^{2+} + 2SO_4^{2-} + 2H^+\,. \qquad \text{(Equation 4-2)}$$

The dissolution produces iron, protons and sulphate. All Fe^{2+} is speciated into cation exchange sites and consequently no goethite precipitation occurs. I.e. goethite neither occurs in the redox front nor in the anoxic side of the calculation column. Since redox drops to reducing levels, part of the produced SO_4^{2-} is further speciated to HS^-. The production of protons is reflected as a drop in pH. Because pH values are low already in the oxic side of the column, only small additional drop in pH is visible in Figure 4-2.

The oxic side (10 000 years, 20 000 years, and 40 000 years) of calculation column behaves in a counterbalancing manner considering goethite (Fig. 4-2). In the oxic proximal parts of the calculation column, infiltrating water releases ferrous iron form the cation exchange sites and causes ferric iron (goethite) precipitation into the column cells. Around 60 mmol/cell of iron is released from the exchange sites and consequently about 60 mmol/cell of goethite is precipitated (cf. Eq. 4-1). Goethite precipitation causes a slight rise in pH values that remains constant until pyrite front is reached within the column.

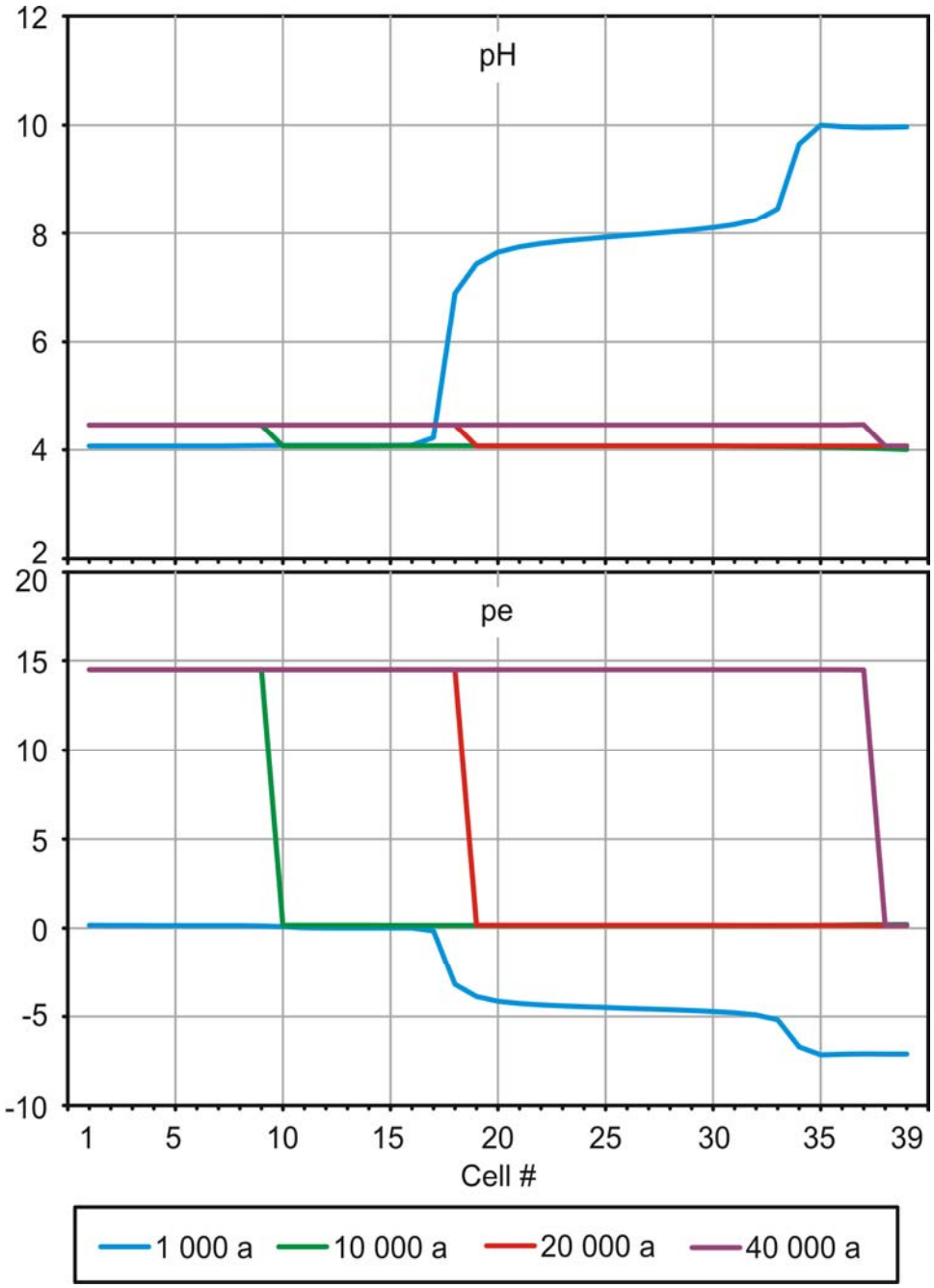

Figure 4-2. *pH and redox conditions within the calculation column at selected 1 000, 10 000, 20 000, and 40 000 years time steps.*

The redox changes occurring in the calculation column are mostly driven by pyrite dissolution. The movement of pyrite front within the calculation column as a function of time is presented in the lower right diagram of Figure 4-3. The pyrite diagram shows that after 40 000 simulated years oxic infiltrating is almost capable pass through the complete calculation column. Dissolved oxygen is consumed away in the cell #38 (5.3m). Redox conditions change abruptly, and this has important consequences for uranium transportation.

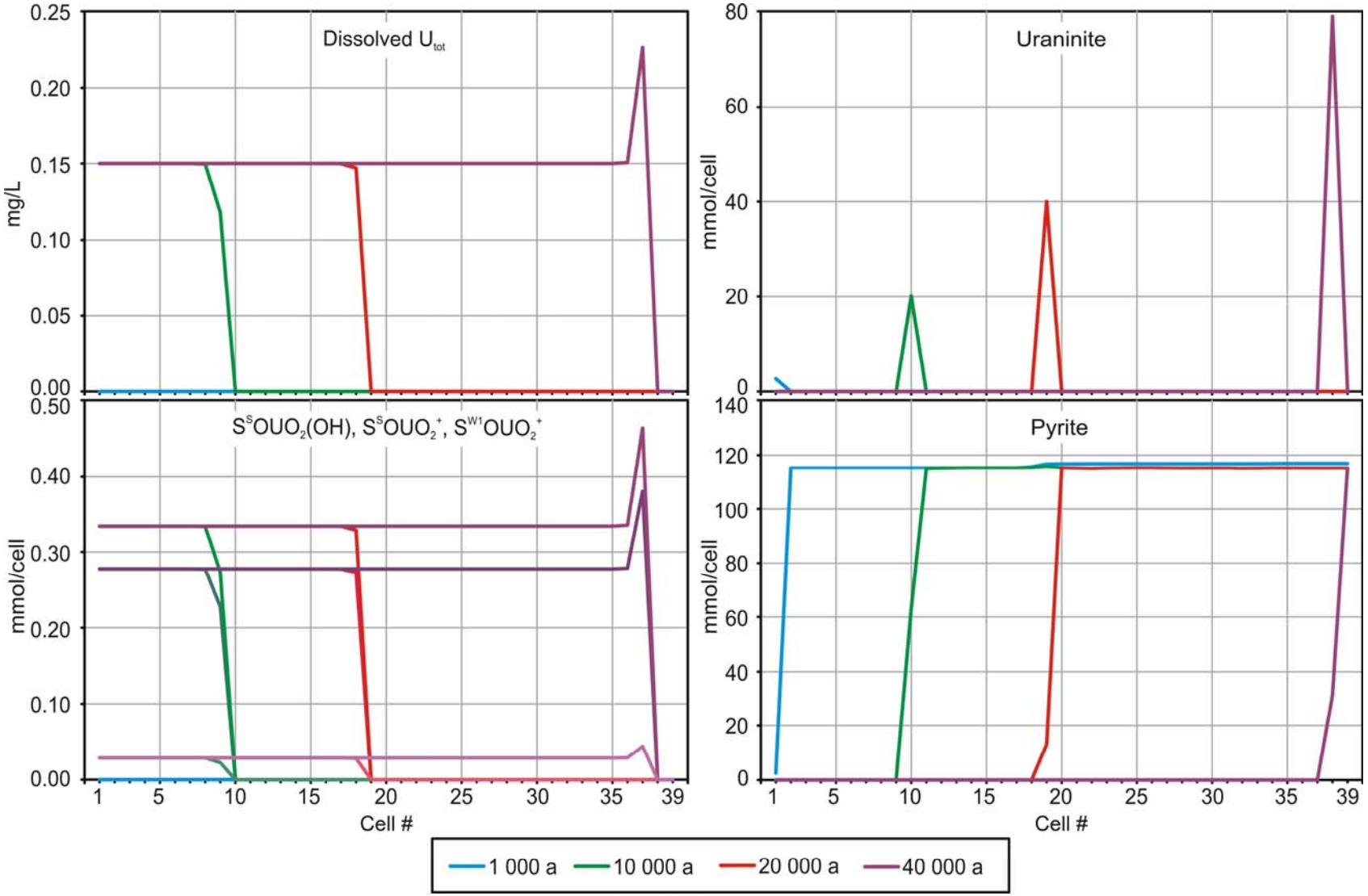

Figure 4-3. *Aqueous and surface complexated uranium (U^{6+}) and evolution of uraninite and pyrite solid phased within the calculation column at selected 1 000, 10 000, 20 000, and 40 000 years time steps.*

Uranium is soluble and readily transportable in its oxidized U^{6+} state (e.g. Brookins 1987). If redox environment for some reason changes to reducing condition, uranium effectively precipitates as uraninite and other uranium minerals. Phenomenon is widely known and used e.g. by ore geologists to explain the so called uranium placer deposits. Famous and very profitable gold-uranium deposits (for example Witwatersrand, South Africa, see e.g. Frimmel & Minter 2002) have been interpreted to be formed with this deposition mechanism.

The current calculation exercise imitates its famous natural analogues. The main points of the phenomenon are illustrated in Figures 4-2 and 4-3. As long as there is a moving redox front within the calculation column, no dissolved uranium can be detected in the outflow side of the calculation column. Uranium carried within steadily infiltrating water is precipitated into the pyrite redox front as uraninite. The phenomenon is illustrated in the upper right diagram of Figure 4-3. Uraninite is gradually and practically linearly cumulated at the redox front as a function of time. Detailed observation of diagrams shows that pyrite dissolution, redox drop and uraninite precipitation occur in the same single cell at certain moment of time. Already the next cell on the reducing side exhibits constant low pH conditions without dissolved uranium. The flow rate utilized (4.2L/year) for the calculation column indicates that equilibration step within each cell (1L pore volume) takes 86.9 days. The rate of pyrite dissolution could be a potential rate limiting step considering the calculation setup. However, the present calculations simply assume that pyrite grain size within the backfill mixture is so small and reactive surface area so large that pyrite dissolution can be approximated with equilibrium thermodynamics (cf. Appelo & Postma 2006, p. 456).

The upper left diagram in Figure 4-3 shows the dissolved uranium concentrations in the oxic side of the calculation column. Dissolved uranium concentration remains mostly at constant 0.15 mg/L level (infiltrating input concentration). However, as the redox cell is approached changes in dissolved uranium concentration occur in the cell preceding the actual redox cell. The reason to this phenomenon remains enigmatic since water dispersivity for cells and diffusion coefficients for aqueous species where defined all zero in the calculations. Intuitively, however, preceding cell concentration anomalies make sense. At early stages (≤10 000 years) precipitated uraninite peak is smaller and broader and it can be expected that the gradual dissolved uranium concentration drop reflects this feature. On the other hand, at late stages of simulation precipitated uraninite peak is high and narrow (i.e. very peaked). It is reasonable to assume that some uraninite re-dissolves into water, and rises dissolved uranium concentration just before the actual redox front is met. Evidently, the concentrations of dissolved uranium distributions preceding the redox front and the sharpness of redox front can be affected with dispersivities, diffusivities, oxygen consumption rates and cell size. In real, the dissolved uranium concentration near the redox front at time step e.g. 40 000 years (Fig. 4-3) can be also much higher than the calculations indicate.

The lower left diagram in Figure 4-3 displays the uranium occupation (only three most dominant species presented) within the available surface sites (Table 2-2). The distribution of surface complexation species is pH dependent. In the pH conditions considered (Fig. 4-2), the $\equiv S^{S}OUO_2(OH)$ is the most common uranium species in the surface sites, following in the popularity is $\equiv S^{S}OUO_2^{+}$. The last uranium species worth note is $\equiv S^{W1}OUO_2^{+}$. The rest occur in negligible concentrations. Significant uranium complexation occurs only in the oxic side of the calculation column. Consequently, U^{6+} is the practically only oxidation state that is stuck into surface sites. As soon as the redox front is reached U^{6+} is released from the surface sites and precipitated as uraninite. The cell preceding the actual redox cell exhibit similar changes in complexed uranium concentrations as was noted above for dissolved uranium.

5 CONCLUSIONS

The comparison between lumped distribution coefficient (K_d) calculation and mechanistic reactive transport calculation gives expected results. It is clearly indicated that distribution coefficients tend to be conservative estimates, meaning here that the coefficients predict higher uranium transport than what is probable.

It is, however, quite remarkable how large differences the two methods may give. Uranium is strongly redox sensitive element, and only the oxidised state is extensively soluble. The distribution coefficient calculation indicates that after 1 000 of years, uranium containing water has penetrated into tunnel backfill to about 2-metre depth from the inflow side. The reactive transport calculations, however, still indicate that practically all uranium is precipitated within few tens of centimetres in the inflow side of the tunnel unit. The distribution coefficient calculations indicate complete uranium breakthrough after some 10 000 years and already long before this benchmark significant traces of uranium should be detectable on the outflow side. The reactive transport calculations, however, predict that the breakthrough will occur at some time after 40 000 years of constant flow. Moreover, reactive transport calculations predict that almost nothing can be detected on the outflow side until the breakthrough occurs. Furthermore, when the breakthrough occurs, complete reserve of uranium concentrated into the tunnel backfill is suddenly moving. It is also worth to note that near the redox front dissolved uranium concentrations at late time steps (e.g. 40 000 years) can be also much higher than calculated simulations indicate.

As it has been pointed out, the distribution coefficient approach is unable to take into account geochemical changes that may occur within natural systems. The sensitivity to redox changes is perhaps the most significant but also other changes may affect considerably to nuclide transport. Among important geochemical changes in the systems can be also changes in pH, changes in ionic strength, and competing chemical reactions. Future scenarios for the Olkiluoto nuclear waste repository assign both high and low pH conditions together with ionic strength changes to the engineered barrier system. As an example of other kind of change, soluble U^{6+} is known to co-precipitate with calcite that is sensitive to pH, dissolved carbonate and calcium concentrations. Also ionic strength changes affect the surface complexation and consequently to the charged water layers counterbalancing the charged surfaces. These diffuse double layer structures may cause complex reactive transport within compacted clay systems. However, the present calculations consider only uranium transport and uraninite precipitation, and competing reactions at the surface complexation sites (uranium complexation).

The reactive transport calculations have its problems as well. The validation of model setup and the modelling tool becomes increasingly complicated as the transport problem becomes more complex. As more reaction mechanisms are added, the traceability and verification of results become increasingly cumbersome. Each added mechanism adds its own thermodynamic parameters into calculation and each parameter usually is only an experimental estimate. If the calculation problems are large enough (considering simulation times and/or volumes) the simulation times likely become extensive and may extend the limits of computing time. Therefore, preference between the two approaches (distribution coefficient vs. mechanistic coupling) is hard to give, though the discrepancies between the two can be interesting and some cases even important.

REFERENCES

Appelo, C.A.J. & Postma, D. (1996) Geochemistry, groundwater and pollution. *A.A. Balkema, Rotterdam, Netherlands. 536 p.*

Appelo, C.A.J. & Postma, D. (2006) Geochemistry, groundwater and pollution. 2nd edition. *A.A. Balkema, Leiden, Netherlands. 649 p.*

Börgesson, L & Hernelind, J (1999) Äspö Hard Rock Laboratory. Prototype Repository. Preliminary modelling of the water-saturation phase of the buffer and backfill materials. *Swedish Nuclear Fuel and Waste Management Co (SKB), Stockholm, Sweden. International Progress Report 00-11*: 99p.

Bradbury, MH. & Baeyens, B. (2005) Modelling the sorption of Mn(II), Co(II), Ni(II), Zn(II), Cd(II), Eu(III), Am(III), Sn(IV), Th(IV), Np(V) and U(VI) on montmorillonite: Linear free energy relationships and estimates of surface binding constants for some selected metals and actinides. *Geochimica et Cosmochimica Acta 69, 875–892.*

Bradbury, MH & Baeyens, B (2003) Porewater chemistry in compacted re-saturated MX-80 bentonite. *Journal of Contaminant Hydrology 61*: 329–338.

Bradbury, MH & Baeyens, B (2002) Porewater chemistry in compacted re-saturated MX-80 bentonite: Physico-chemical characterisation and geochemical modelling. *Paul Scherrer Institute, Villingen, Swizerland, PSI Bericht 02-10*: *41 p.*

Brookins, D.G. (1987) Eh-pH diagrams for geochemistry. Springer-Verlag, Berlin. 176 p.

Cedercreutz, J. (2004) Future climate scenarios for Olkiluoto with emphasis on permafrost. *Posiva Oy, Eurajoki, Finland. Report POSIVA 2004-06. 72 p.*

Charlet, L. & Tournassat, C. (2005) Fe(II)–Na(I)–Ca(II) cation exchange on montmorillonite in chloride medium: Evidence for preferential clay adsorption of chloride – Metal ion pairs in seawater. *Aquatic Geochemistry 11, 115–137.*

Davis, JA & Kent, DB (1990) Surface complexation modeling in aqueous geochemistry. In: (ed. Ribbe, P.H.) Mineral-water interface geochemistry. *Mineralogical Society of America, Washington D.C., U.S.A. Reviews in Mineralogy 23*: 177–260.

Frimmel, H.E. & Minter, W.E.L. (2002) Recent developments concerning the geological history and genesis of the Witwatersrand gold deposits, South Africa. In: (eds. R.J. Goldfarb & R.L. Nielsen) Integrated Methods for Discovery: Global Exploration in the 21st Century. Society of Economic Geologists, Special Publication 9. 17–45.

Grenthe, I., Fuger, J., Konings, R.J.M., Lemiere, R.J., Muller, A.B., Nguyen-Trung, C. Wanner, H., & Forest, I. (2004) Chemical thermodynamics of uranium. *Nuclear Energy Agency, OECD, Paris, France. 715 p.*

Nordman, H. & Vieno. T. 1994 Near-field model REPCOM. Nuclear Waste Commission of Finnish Power Companies, Report YJT-94-12.

Parkhurst, D.L. & Appelo, C.A.J. (1999) User's guide to PHREEQC (Version 2) – A computer program for speciation, batch-reaction, one-dimensional transport, and inverse geochemical calculations. *U.S. Geological Survey, Denver, Colorado. Water-Resources Investigations Report 99-4259*: 312 p.

Posiva (2007) Expected evolution of a spent fuel repository at Olkiluoto. *Posiva Oy, Helsinki, Finland. Report POSIVA 2006-05. 412 p.*

SKB (2005) Äspö Hard Rock Laboratory. Annual Report 2004. *Swedish Nuclear Fuel and Waste Management Co (SKB), Stockholm, Sweden. Technical Report TR-05-10. 211 p.*

Vuorinen, U., Lehikoinen, J., Luukkonen, A. & Ervanne, H. (2003) Effects of salinity and high pH in crushed rock and bentonite - experimental work and modelling in 2001 and 2002. *Posiva Oy, Eurajoki, Finland. Working Report 2003-22, 33 p.*